2011 American Control Conference
on O'Farrell Street, San Francisco, CA, USA
June 29 - July 01, 2011

Design, Prototyping, Modeling and Control of a MEMS Nanopositioning Stage

Y. Zhu, *Member, IEEE*, A. Bazaei, S. O. R. Moheimani, *Fellow, IEEE*, and M. R. Yuce, *Senior Member, IEEE*

Abstract— **In this paper, real-time feedback control of a novel micro-machined 1-degree-of-freedom (1-DoF) thermal nanopositioner with on-chip electrothermal positioning sensors is presented. The actuation works based on thermal expansion of silicon beams. The sensing mechanism works based on the difference between the electrical resistances of two electrically biased identical Silicon beams. The difference increases with displacement as the heat conductance of the sensor beams vary oppositely with position, resulting in different beam temperatures and resistances. The sensor pair is operated in a differential way to reduce low-frequency drift. The nanopositioner has a nonlinear static input-output characteristic. An open-loop control system is first designed using polynomials that approximately compensate the nonlinear characteristics. It is experimentally shown that plant uncertainties and sensor drift result in unacceptable performance for open-loop control of the thermal nanopositioner. Hence, feedback control methods are necessary for accurate nanopositioning. A closed-loop feedback control system was then designed using a proportional-integral (PI) controller and the nonlinear compensator used for the open-loop control system. The closed-loop system provides acceptable and robust tracking performance for a wide range of set point values. For triangular reference tracking, which is needed in raster-scanned SPM, the tracking performance of the closed-loop system is further improved by incorporating a suitable pre-filter.**

Index Terms-Thermal actuation, thermal position sensing, microelectromechanical system (MEMS), nanopositioning, feedback control.

I. Introduction

High precision nanopositioners have been used extensively in many applications such as scanning probe microscopy (SPM) [1], atomic force microscopy (AFM) [2], and emerging ultrahigh density probe storage system [3, 4]. Although macro-scale nanopositioners can achieve nanometer-scale positioning resolution and accuracy, they are relatively large and expensive [5, 6]. Microelectromechanical System (MEMS) nanopositioners have attracted increasing research interest recently due to their small size, low cost, and highly parallel nanoscale manipulation and assembly strategies [7]. Closed-loop feedback control of the positioners is highly desirable if a high degree of displacement precision is required, and such a control system needs an accurate source of position information [8]. However, many of the MEMS nanopositioners reported in the literature have no on-chip sensors due to the restrictions associated with micro-fabrication processes [9]. Thus, the in-plane movements are often measured by laser reflectance microscopes [10, 11] or optical microscopes [12], making the footprint of the whole system fairly large. There are several exceptions in the literature, for example, an embedded on-chip capacitive displacement sensor was integrated in a thermally actuated positioner in [13]. Nevertheless, only open-loop results were obtained, and a complex fabrication process was required for electrical insulation between electrical heating and sensing circuits. Recently, a thermal sensing scheme was used in a probe-based storage device [14]. Micro-heaters were used to measure the motion of a MEMS micro-scanner with resolution of less than 1 nm. Compared to a comb capacitive sensor, a thermal sensor is more compact and can be easily integrated with actuators in a MEMS device. In [15, 16], off-chip electromagnetic coil actuators were adopted for scanner actuation, and a complex mass-balanced structure was designed for vibration resistance purposes.

In this paper, a novel electrothermal position sensor is integrated with a thermal actuator in the same MEMS chip without the need for inclusion of extra electrical insulation fabrication process as reported in [13], or assembling two chips as reported in [15]. Compared to other MEMS actuation mechanisms, the thermal actuators have advantages of low voltage operation, large forces, and a high vibration resistance due to their stiff structures [17]. A MEMS device with integrated electrothermal actuation and sensing has been micro-fabricated in a bulk silicon process. To reduce the low frequency thermal drift, the sensors are operated in a pair and measured by a differential circuitry. The on-chip displacement sensing enables a feedback control capability. A model of the positioner is derived and a proportional-integral (PI) feedback controller is implemented digitally in a dSPACE rapid prototyping system to investigate the closed-loop performance of the positioner. Open-loop and closed-loop step displacement tracking were investigated. The closed-loop step response results show a positioning resolution of 7.9 nm and a time constant of 1.6 ms, while the

Manuscript received September 28, 2010. This research was funded by Australian Research Council (ARC) discovery grant- DP0774287.

Y.Zhu is with the School of Engineering, Griffith University, Australia (email: y.zhu@griffith.edu.au).

A.Bazaei, S.O.R.Moheimani, and M.R.Yuce are with the School of Electrical Engineering and Computer Science, the University of Newcastle, Australia (email: {ali.bazaei, reza.moheimani, mehmet.yuce} @newcastle.edu.au).

open-loop seek operation resulted in a maximum positioning error of 620 nm. Good tracking performance was also obtained for a 10 Hz triangular reference by using a 2-DoF feedback control system consisting of a PI controller and a pre-filter.

II. Design

The conceptual schematic view of the nanopositioner is presented in Fig.1. The device is micro-fabricated from single-crystal silicon using a commercial bulk silicon micromachining technology-SOIMUMP in MEMSCAP. This process has a 25 µm thick silicon device layer and a minimum feature/gap of 2 µm. The Scanning Electron Microscope (SEM) image of the whole device and a section of it are provided in Fig.2. The position sensors are two beam-shaped resistive heaters made from doped silicon. Application of a fixed dc voltage across the heaters results in a current passing through them, thereby heating the beams. As a heat sink, a rectangular plate is placed beside the beam heaters with a 2 µm air gap. The positioner stage is actuated by a thermal actuator, as illustrated in Fig.2.

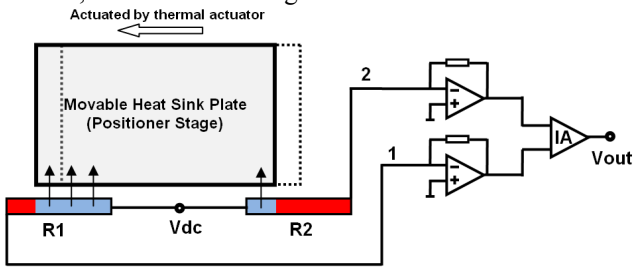

Fig. 1. Schematic diagram of the thermal position sensor with a differential amplifier circuit.

Before applying a voltage across the actuator, the positioner stage is at the initial rest position (dashed box in Fig.1), where the two edges of the sink plate are exactly aligned with the middle of the two thermal resistive sensors R_1 and R_2. The sensors are biased by a dc voltage source V_{dc}, and the heat generated in the resistive heater is conducted through the air to the heat sink plate (positioner stage). As the plate is centered between the two thermal sensors, the heat fluxes out of the sensors are identical, thereby equaling the temperature and resistance of the sensors. After applying a voltage on the actuator beams, the positioner stage is displaced towards left. The heat fluxes associated with the sensors on the left and on the right are becoming different, resulting in a corresponding difference in the resistance of the left sensor (R_1), and the right sensor (R_2). Thus, the displacement information of the positioner stage can be detected by measuring the resistance difference between the two sensors. The differential changes of the resistance result in current variations in the beam resistors, and the currents are converted to an output voltage using a pair of trans-impedance amplifiers and an instrumentation amplifier. To suppress the common-mode noise, the gains of these two trans-impedance amplifiers must be well matched by adjusting the feedback resistance of the trans-impedance amplifiers. Employing the differential topology allows the sensor output to be immune from undesirable drift effects due to changes in ambient temperature or aging effects.

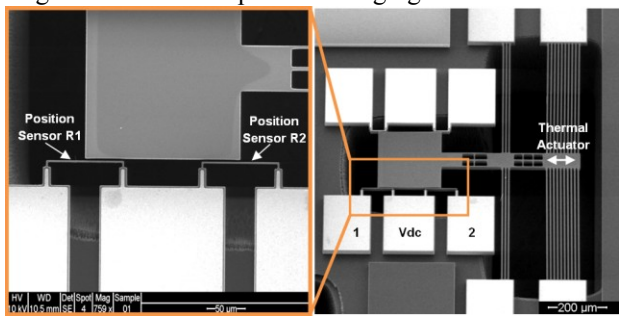

Fig.2. SEM images of the micromachined nanopositioner

The positioner stage is actuated by a chevron thermal actuator, as illustrated in Fig.2. Compared to other actuation methods, the thermal actuators are simple to implement, operate at low voltage, and provide large forces. Due to the stiffness of the structures, no complex mass-balanced structures are needed for vibration resistance purposes, as proposed in [16]. The chevron thermal actuator has two pairs of thin hot arms at a small angle with respect to each other as shown in Fig.2, and the dimensions are listed in Table I. The chevron actuator's operating voltage range is typically 0 to 15 V, depending on the geometry. The displacement is proportional to V^2, and the maximum displacement is limited by buckling of the hot arms at high temperatures (>700 ºC) [11].

To reduce the thermal coupling effects from the thermal actuators to thermal sensors, a number of holes were made in the centre shuttle between actuators and the heat sink plate. The holes are expected to improve the thermal convection, thereby thermally insulating the heat sink plate from actuators. The suspension beams help the thermal insulation as well, due to the heat can transfer to the substrate through the suspension beams and its anchors.

III. Modeling

In this section, we predict the sensor temperature and resistance as a function of sensor bias and actuator displacement. To simplify the analysis, lumped parameter approach and static conditions are considered here. This means we assume a uniform temperature distribution in each sensing resistor. The following discussion shows how lumped parameter analysis can predict the temperature in terms of the applied voltage.

Let the electric resistance of a resistor at room temperature T_o be R_o (Ω) and its variation with temperature is described by a constant temperature coefficient α (1/ºC). The overall thermal conductance between the resistor and the outside world, including its connection to a voltage source, is K (W/ºC). Assuming a uniform temperature distribution T across the resistor, we can equate the electric power generat-

ed in the resistor with the thermal power flow from the resistor to the outside world as:

$$\frac{V^2}{R_o[1+\alpha(T-T_o)]} = K(T-T_o) \tag{1}$$

where V is the constant voltage across the resistor. Since the constant α does not depend on temperature, the resistance value and its temperature can be formulated in the following form:

$$R = R_o \frac{1+\sqrt{1+\frac{4\alpha V^2}{R_o K}}}{2} \tag{2}$$

$$T = T_o + \frac{\sqrt{1+\frac{4\alpha V^2}{R_o K}}-1}{2\alpha} \tag{3}$$

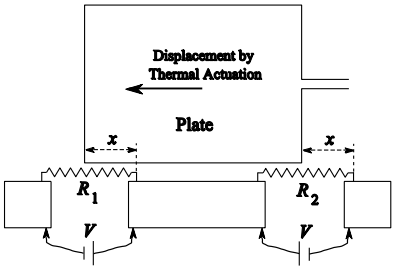

Fig. 3. Schematic diagram of the biased thermal sensors.

Referring to Fig. 3, let us define K_1 and K_2 as the overall thermal conductance from electric resistors R_1 and R_2 of the sensor to the area around the sensor, respectively. As the plate in Fig. 3 moves to the left side, K_1 increases while K_2 decreases. Let us assume a simple dependency between the thermal conductance and the plate position x, defined in Fig. 3, in the following forms:

$$K_1(\tilde{x}) = K_{\min} + (K_{\max} - K_{\min})\tilde{x},$$
$$K_2(\tilde{x}) = K_{\min} + (K_{\max} - K_{\min})(1-\tilde{x}) \tag{4}$$

where $\tilde{x} \equiv x/L$ is the normalized position, L is the length of each resistor, and K_{min} and K_{max} refer to minimum and maximum thermal conductance of each resistor. In this way, Equations (2) and (3) can be used to predict the steady-state values of resistors and their temperatures in the following form:

$$R_i(\tilde{x},V) = R_o \frac{1+\sqrt{1+\frac{4\alpha V^2}{R_o K_i(\tilde{x})}}}{2},$$
$$T_i(\tilde{x},V) = T_o + \frac{\sqrt{1+\frac{4\alpha V^2}{R_o K_i(\tilde{x})}}-1}{2\alpha}, \quad i \in \{1,2\} \tag{5}$$

where R_o is each resistance value at zero bias voltage. At zero actuation, where $\tilde{x} = 0.5$ and $K_1 = K_2 = (K_{\max} + K_{\min})/2$, we assume that the sensor resistors match. Hence, the sensor output voltage is proportional to $R_1^{-1} - R_2^{-1}$. We employ this difference between electric conductances to measure the displacement as illustrated in the following simulation.

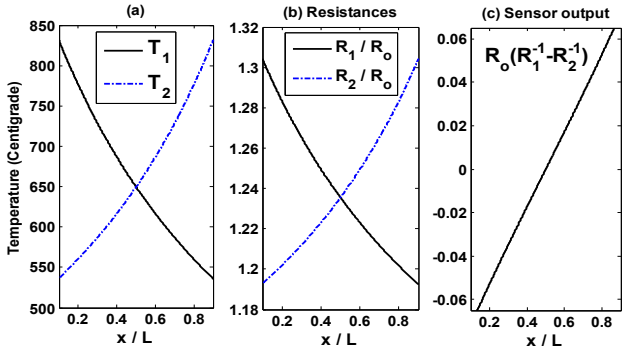

Fig.4. Steady-state values versus displacement for (a) resistor temperatures, (b) resistor values, and (c) normalized sensor output.

Assuming the parameter values in Table I and using Equations (4) and (5), the steady-state values of temperatures, resistances, and sensor output for different position values are obtained as shown in Fig. 4(a)-(c), respectively. Although the resistance values depend nonlinearly on displacement, the sensor output exhibits an almost linear dependency on displacement.

TABLE I.

PARAMETER VALUES FOR SIMULATION

Parameter	Value
α (K^{-1})	3.7822×10^{-4}
R_o (Ω)	390
T_o (°C)	27
K_{min} (W/K)	8×10^{-5}
K_{max} (W/K)	16×10^{-5}
V (V)	6

IV. CONTROL

In this section, open-loop and closed-loop position control strategies are investigated for the positioner. A dSPACE-1103 rapid prototyping system was used for real time implementation of the controllers and data acquisition.

A. Open-loop control

With a sensor bias voltage of 7V, an open-loop test was performed where a slowly varying trapezoidal voltage in the range of 0-9V was applied to the actuator (using dSPACE). Fig.5 shows the waveforms. The sensor has a small offset at zero actuation. After cancelling the sensor offset, the observed sensor output response to actuation input can be described by the output-input stationary characteristic shown in Fig.6.

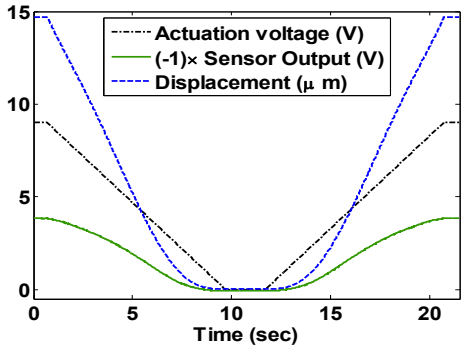

Fig.5. Open-loop response of thermal positioner to a slowly varying trapezoidal actuation.

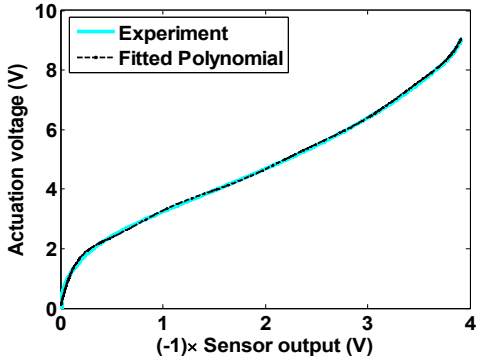

Fig.6. Output-input stationary characteristic ($P_1(\cdot)$).

To generate this characteristic, we used the rising portion of the experimental trapezoidal data. A nonlinear mapping was obtained by fitting a ninth order polynomial to the experimental output-input characteristic, shown in Fig.6. As shown in Fig. 7, mapping $P_1(\cdot)$ is used in series with the actuation for compensation of the nonlinearity in the static input-output characteristic.

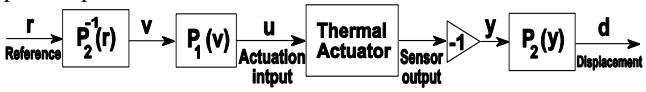

Fig.7. Block diagram of the open-loop controller.

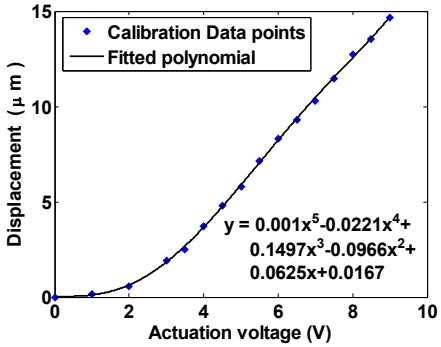

Fig.8. Nonlinear mapping from actuation to displacement using calibration data.

To convert the sensor output voltage to displacement, a fifth order polynomial was fitted to the calibration data obtained by PMA. The polynomial along with the calibration data points are shown in Fig. 8. Using this polynomial, a displacement data corresponding to the trapezoidal actuation voltage is obtained and displayed in Fig. 5 with the dashed line.

Having obtained the displacement data, a static displacement characteristic can be generated for the sensor as shown in Fig. 9 (the rising portion of the data in Fig. 5 was used with the sensor offset cancelled). As shown in Fig. 9, another nonlinear mapping is obtained by fitting a seventh order polynomial to the experimental sensor characteristics. This mapping, which is used for online approximation of the displacement using the sensor signal, is described as:

$$d = P_2(y) = 0.023y^7 - 0.2727y^6 + 1.2394y^5 - 2.688y^4 + 2.8588y^3 - 1.0242y^2 + 2.1020y - 0.0048$$

where d is the displacement in μm and y is the sensor signal in volts multiplied by (-1) after offset cancellation.

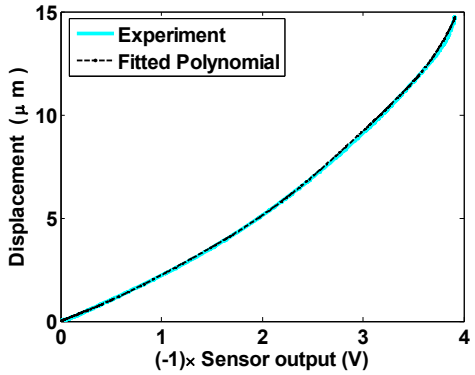

Fig.9. Static displacement-sensor characteristic ($P_2(\cdot)$).

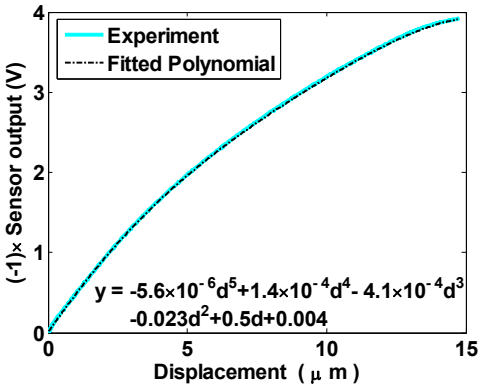

Fig.10. Static sensor-displacement characteristic ($P_2^{-1}(\cdot)$).

In order to map a desired displacement to its corresponding sensor signal value, a fifth order polynomial, denoted by $P_2^{-1}(r)$ in Fig. 7, was fitted to the experimental sensor-displacement characteristic, as shown in Fig. 10. For open-loop control we use the nonlinear mappings $P_1(\cdot)$ and $P_2^{-1}(\cdot)$, as shown in Fig. 7, to compensate for system nonlinearities. Using a sample and hold block, the sensor offset is automatically cancelled before applying the actuation voltage. As shown in Fig. 11 with a stair case reference signal, the open-loop control method cannot provide an acceptable tracking performance for displacement. This is due to plant uncertainties and sensor drift. Hence feedback control is

necessary for accurate positioning.

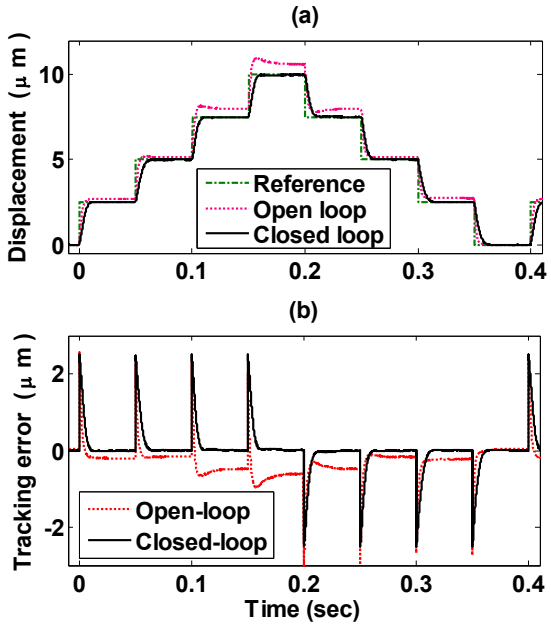

Fig.11. Closed-loop and open-loop experimental results for 0, 2.5, 5, 7.5 and 10 μm seek operations. (a) Displacements, (b) Tracking errors.

B. Closed-loop control

For closed-loop control, we incorporated a PI controller in addition to the nonlinear mappings, as shown in Fig. 12. The integration part in PI controller provides a closed-loop unity low frequency gain form reference to displacement for set-point tracking and robustness to uncertainties and disturbances. The proportional part in the PI controller is used to reduce overshoot in step response. With an integral gain of ki=250 and a proportional gain of kp=0.2, the positioning performance is significantly improved as shown in Fig. 11. Based on this control scheme, a controllable desired response of 2.5 μm steps over a 10 μm range was obtained with a time constant of 1.6 ms, as illustrated in Fig.11. As a comparison, a similar open-loop seek operation resulted in a maximum positioning error of 0.62 μm.

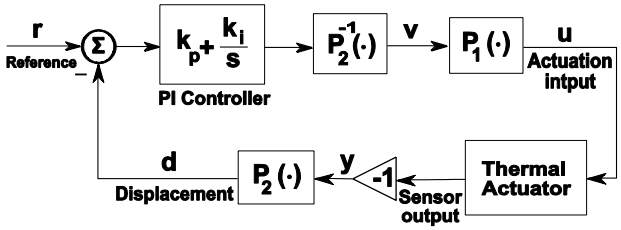

Fig.12. Block diagram of the closed-loop PI controller.

For triangular reference tracking, we used a 2-degree-of-freedom control system as shown in Fig. 13. The 2DoF control system consists of a PI controller and a pre-filter (the nonlinear mappings are as before). To provide more stability margins we used lower gains of ki=130 and kp=0.16 for the PI controller. This is also useful to reduce effect of measurement noise on the controlled displacement output due to feedback. The pre-filter with the frequency response shown in Fig. 14, is used to speed up the response and reduce the tracking error without affecting the stability margins and unity low-frequency gain of the closed-loop system. The tracking performance for a 10Hz triangular reference is shown in Fig. 15. It is seen that displacement output closely follows a desired triangular reference within a wide range of 10 μm with a standard deviation of 0.18 μm.

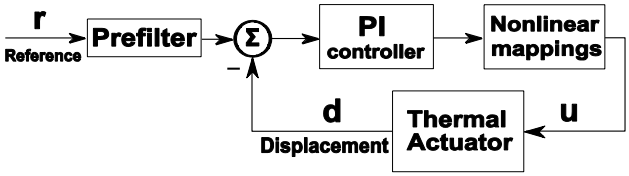

Fig.13. Two-degree-of-freedom feedback control structure.

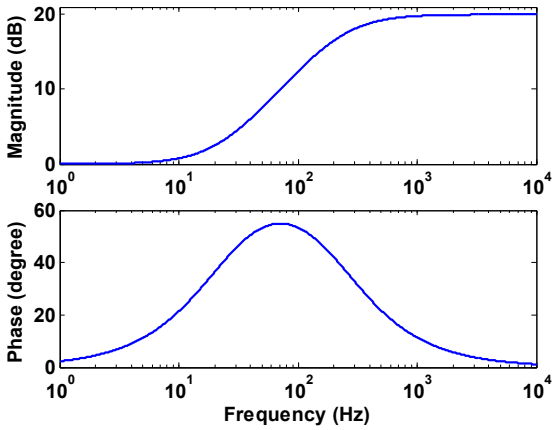

Fig.14. Bode diagram of pre-filter in 2-DoF control system.

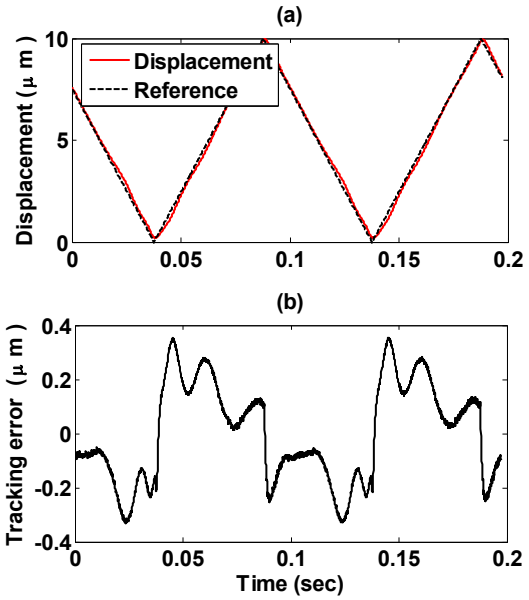

Fig.15. Triangular reference tracking by 2-DoF feedback control system.

V. CONCLUSION

A novel micromachined silicon nanopositioner with on-chip thermal actuator and sensor has been presented with nanometer resolution and low sensor drift. The MEMS positioner was embedded in a feedback loop to realize a precise position control. Due to the nonlinear nature of the thermal actuator, a nonlinear inversion block was added to the feedback loop to linearize the plant. The experimental results showed that the positioner with the PI controller achieved a high degree of positioning accuracy with very good robustness. Due to the limitation of the SOIMUMPs fabrication process, it is not possible to design a two-dimensional thermal based positioner in a single device layer. However, the thermal sensors and actuators can be placed in different layers, which can be fabricated in METALMUMPs process through MEMSCAP. A 2DOF thermal based nanopositioner is under investigation by the authors for imagining applications.

REFERENCES

[1] G.Binning, and H.Rohrer, "The scanning tunneling microscope," *Sci.Am.,* vol.253, pp.50-56, 1986.

[2] G.Binning, C.Quate, and C.Gerber, "Atomic force microscope," *Phys. Rev. Lett.*, vol.56, no.9, pp.930-933, 1986.

[3] N.B.Hubbard, M.L.Culpepper, and L.L.Howell, "Actuators for micropositioners and nanopositioners," *Transactions of the ASME*, Vol.59 November 2006, pp.324-334.

[4] A.Pantazi, M.A.Lantz, G.Cherubini, and H.Pozidis, and E.Eleftheriou, "A servomechanism for a micro-electro-mechanical-system-based scanning-probe data storage device," *Nanotechonology*, 15, pp.S612-S621, 2004

[5] Y.K.Yong, S.S.Aphale, and S.O.R.Moheimani, "Design, Identification, and Control of a Flexure-Based XY Stage for Fast Nanoscale Positioning," *IEEE Trans. on Nanotechnology*, Vol.8, No.1, pp.46-54, 2009.

[6] Y.K.Yong, S.S.Aphale, and S.O.R.Moheimani, "Atomic force microscopy with a 12-electrode piezoelectric tube scanner," *Review of Scientific Instruments*, Vol.81, No.3, pp033701, 2010.

[7] C.H.Kim, and Y.K.Kim, "Micro XY-stage using silicon on a glass substrate," *J.Micromech. Microeng.,* Vol.12, pp.103-107, 2002.

[8] S.Devasia, E.Eleftheriou, and S.O.R.Moheimani, "A survey of control issues in nanopositioning," *IEEE Trans. on control systems technology*, vol.15, no.5, 2007, pp.802-823

[9] K.Gum, X.X.Li, H.Bao, B.Liu, Y.Wang, M.Liu, Z.Yang, and B.Cheng, "Single wafer processed nanopositioning XY-stage with trench-sidewall micromaching technology," *J.Micromech.Microeng*., Vol.16, pp.1349-1357, 2006.

[10] J.J. Gorman, Y-S. Kim, and N.G. Dagalakis, "Control of MEMS nanopositioners with nano-scale resolution," *Proceeding of IMECE2006*, Chicago, IIIinois USA, November 5-10, 2006.

[11] R.Hichey, D.Sameoto, T.Hubbard, and M.Kujath, "Time and frequency response of two-arm micromachined thermal actuators", *J.Micromech.Microeng.*, 13, (2003), pp.40-46.

[12] Y.Sun, M.A.Greminger, D.P.Potasek, and B.J.Nelson, "A Visually Servoed MEMS Manipulator," *Experimental Robotics VIII*, Springer Berlin/Heidelberg, 2003, pp.255-264.

[13] L.L. Chu, and Y.B. Gianchandani, "A micromachined 2D positioner with electrothermal actuation and sub-nanometer capacitive sensing", *J. Micromech. Microeng.*, 13 (2003), pp.279-285.

[14] M.A.Lantz, G.K.Binning, M.Despont, and U.Drechsler, "A micromechanical thermal displacement sensor with nanometre resolution," *Nanotechnology*, 16 (2005), pp.1089-1094.

[15] A.Sebastian, A.Pantazi, S.O.R. Moheimani, H.Pozidis, and E.Eleftheriou, "Achieving subnanometer precision in a MEMS-based storage device during self-servo write process," IEEE Tran. on nanotechnology, vol.7, no.5, 2008, pp.586-595

[16] M.A.Lantz,, H.E.Rothuizen, U.Drechsler, W.Haberle, and M.Despont, "A vibration resistant nanopostioner for mobile parallel-probe stroage applications," J. microelectromechanical systems, vol.16, no1, 2007, pp.130-139.

[17] V.Kaajakari, *Practical MEMS*. Las Vegas, NV: Small Gear Publishing, 2009.